Hue University Journal of Science: Natural Science
Vol. 130, No. 1D, 5–14, 2021

pISSN 1859-1388
eISSN 2615-9678

MODEL PREDICTIVE DIRECT POWER CONTROL OF THREE-LEVEL T-type INVERTER-FED DOUBLY-FED INDUCTION GENERATOR FOR WIND ENERGY SYSTEM

Ngo Van Quang Binh[1*], Nguyen Khanh Quang[2], Nguyen Tu Ha[1], Hoang Dinh Long[1], Dao Quoc Chinh[3]

[1] Faculty of Physics, University of Education, Hue University, 34 Le Loi St., Hue, Vietnam
[2] University of Science and Technology, The University of Danang, 54 Nguyen Luong Bang St., Lien Chieu, Da Nang, Vietnam
[3] Department of electrical and electronic engineering, Hue Industrial College, 70 Nguyen Hue St., Hue, Vietnam

* Corresponding author: Ngo Van Quang Binh <nvqbinh@hueuni.edu.vn>

(*Received: 16 May 2021; Accepted: 26 May 2021*)

Abstract. The paper proposes a simplified direct power control strategy of a doubly-fed induction generator fed by a three-level T-type inverter based on finite control set model predictive control. A mathematical model based on grid voltage orientation was employed to determine the predictive values of the stator flux, rotor current, and capacitor voltages for all feasible rotor-side inverter output voltages. The active and reactive powers were calculated by using the grid voltage and the rotor current. A cost function was applied to track the active and reactive powers, maintain the balance of capacitor voltages, and reduce the common-mode voltage. The best switching control input was chosen by minimizing the cost function and implemented to the inverter. Different operating conditions of wind turbine systems were studied with Matlab/Simulink environment. The simulation results validate the improved performance of the proposed method compared with the classical control in terms of transient response and steady-state conditions.

Keywords: doubly-fed induction generator, DFIG, three-level T-type inverter, finite control set model predictive control, FCS-MPC, direct power control, capacitor voltage balancing, wind energy system

Nomenclature

ω_s, ω_m : synchronous, rotor, and slip angular frequencies

ψ_s, ψ_r : stator, rotor flux linkage vectors

θ_r : angle between the rotor frame and stator voltage frame

θ_s, θ_m : stator voltage and rotor angles

$\sigma = 1 - L_m^2 / L_s L_r$: coefficient of leakage

C_1, C_2, C : capacitance of the dc-link

i_s, i_r : stator and rotor current vectors

: inductance of the stator and rotor windings

$L_{s\sigma}, L_{r\sigma}$ L_s, L_r, L_m : stator, rotor self-inductance and mutual inductance

P_g, Q_g : grid active and reactive powers

P_r, Q_r : rotor active and reactive powers

P_s, Q_s : stator active and reactive powers

R_s, R_r : resistances of the stator and rotor windings

s : the slip of machine

$\mathrm{T}_s = L_s / R_s$: time constant of the stator winding

T_{sp} : sampling time of the controller

U_{dc} : dc-bus voltage

u_s, u_r : stator and rotor voltage vectors

superscripts

* : reference value

dq: stator voltage reference frame

DQ: rotor reference frame

p: predicted value

1 Introduction

Nowadays, wind energy has been recognized as a sustainable resource for power generation systems thanks to its benefits, such as lower carbon emissions and decreased air pollution. Major wind turbine production is within the 1.5–6 MW rating. Meanwhile, a doubly-fed induction generator (DFIG) depicts a feasible solution due to its attractiveness: reduce power converter about 30% of the generator power and allow bi-directional power transmission through a back-to-back converter (Fig. 1) [1-4]. A T-type inverter has satisfying performance in terms of high capacity, reduction in common-mode voltage (CMV), and low harmonic distortion of the inverter output voltage and current [4, 5]. Several methods were proposed to solve the main limitation of the capacitor voltage unbalancing. Consequently, the T-type inverters are extensively utilized in high power conversion systems.

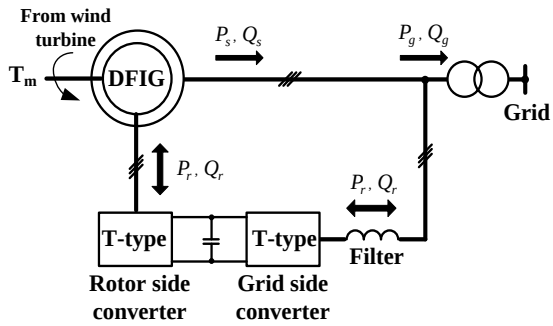

Fig. 1. Wind energy conversion systems based on DFIG

A well-known method is applied to control the DFIG wind energy conversion system based on the stator flux orientation (SFO) and stator voltage orientation (SVO) [6-8]. However, the disadvantages of the SFO are the limit of the reactive power flow due to the stability and the complex stator flux angle. In the SVO, the active and reactive powers can be controlled via a proportional-integral (PI) stator current control loop. Nevertheless, the accuracy of the tuning gains of PI controllers and DFIG's parameters affects control system performance. Recently, a direct power control (DPC) has been proposed to improve the control system performance. This method uses a hysteresis control and a lookup table to directly control the stator active and reactive powers [9-11]. Nonetheless, this method requires a short sampling time to obtain adequate control performance. It is not easy to further handle constraints such as capacitor voltage balancing and reducing the CMV with linear and hysteresis control approaches. In the last few years, the finite control set model predictive control (FCS-MPC) has been considered as an attractive solution for power electronic applications due to its numerous benefits, such as simple control strategy, easy incorporation of nonlinearity, additional constraint, and computation time [12-19]. Further, the predictive control achieves acceptable transient and steady-

pISSN 1859-1388
eISSN 2615-9678

state conditions in comparison with the classical technique.

In this paper, a simplified direct power control strategy based on FCS-MPC is proposed to carry out the DFIG fed by a three-level T-type inverter. The suggested approach permits regulating the generated active and reactive powers, keeping the balance of capacitor voltages, and decreasing the CMV. A dynamic model based on a grid voltage orientation is employed to predict the behaviour of stator, rotor currents, and DC-link capacitor voltages for all feasible switching control inputs. An appropriate cost function is used to achieve the control objectives. The best switching state via optimizing cost function is applied to the inverter, eliminating the modulation block and cascade control loops. Furthermore, a two-step horizon is utilized to improve the control performance and compensate for the computational delay. The simulation results confirm the improved performance of the proposed control strategy in terms of transient and steady-state operation and neutral point voltages deviation compared with the classical control method. Additionally, the CMV is reduced with an appropriate weighting factor in the cost function, leading to a more extended machine operating life.

The rest of the paper is organized as follows: Section 2 introduces the mathematical model of the DFIG fed by a 3L-T-type inverter. The following section details the proposed control strategy based on the finite control set model predictive control approach. In Section 4, a comparative investigation between the proposed method and the conventional method is analyzed with simulation results. Our conclusions are drawn in the final section.

2 Mathematical model of DFIG fed by a 3L-T-type inverter

The equivalent circuit of the DFIG in the stator voltage-orientated reference frame is presented in Fig. 2. The mathematical model of the DFIG in the synchronous reference frame (dq) is given by [3]

$$u_s^{dq} = R_s i_s^{dq} + \frac{d\psi_s^{dq}}{dt} + j\omega_s \psi_s^{dq} \quad (1)$$

$$u_r^{dq} = R_s i_r^{dq} + \frac{d\psi_r^{dq}}{dt} + j(\omega_s - \omega_m)\psi_r^{dq}$$

The fluxes are expressed via the stator and rotor currents as

$$\psi_s^{dq} = L_s i_s^{dq} + L_m i_r^{dq} \quad (2)$$

$$\psi_r^{dq} = L_r i_r^{dq} + L_m i_s^{dq}$$

The voltage components in the stator voltage reference frame (Fig. 3) can be assumed as

$$u_{ds} = U_g; u_{qs} = 0 \quad (3)$$

where U_g denotes the magnitude of the grid voltage that can be determined by using a phase-locked loop.

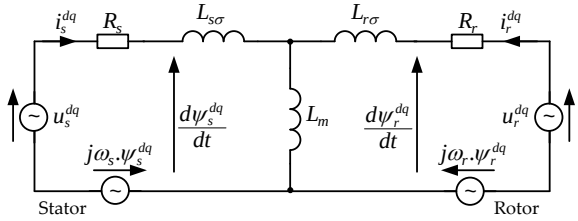

Fig. 2. Equivalent dynamic diagram of the DFIG in a dq coordinate reference frame

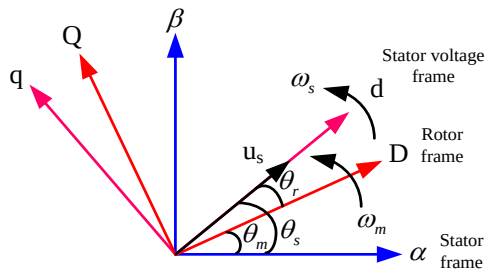

Fig. 3. Coordinate reference frame for control DFIG

Combining (1), (2), and (3) gives the reduced state space representation of the dynamic model for the DFIG as

$$\dot{x} = A(\omega_s, \omega_m)x + Bu \tag{4}$$

where $x = \begin{bmatrix} i_{ds} \\ i_{qs} \\ i_{dr} \\ i_{qr} \end{bmatrix}, u = \begin{bmatrix} u_{ds} \\ u_{dr} \\ u_{qr} \end{bmatrix},$

$$A = \frac{1}{\sigma L_s L_r}\begin{bmatrix} A_{11} & A_{12} & A_{13} & A_{14} \\ A_{21} & A_{22} & A_{23} & A_{24} \\ A_{31} & A_{32} & A_{33} & A_{34} \\ A_{41} & A_{42} & A_{43} & A_{44} \end{bmatrix},$$

$$A_{11} = -R_s L_r, A_{12} = \omega_m L_m^2 + \omega_s \sigma L_s L_r, A_{13} = R_r L_m$$

$$A_{14} = \omega_m L_m L_r, A_{21} = -A_{12}, A_{22} = A_{11}, A_{23} = -A_{14}$$

$$A_{24} = A_{13}, A_{31} = R_s L_m, A_{32} = \omega_m L_s L_m,$$
$$A_{33} = -R_r L_s, A_{34} = -\omega_m L_s L_r + \omega_s \sigma L_s L_r,$$

$$A_{41} = A_{32}, A_{42} = A_{31}, A_{43} = -A_{34}, A_{44} = A_{33}$$

$$B = \frac{1}{\sigma L_s L_r}\begin{bmatrix} L_m & -L_m & 0 \\ 0 & 0 & -L_m \\ -L_m & L_s & 0 \\ 0 & 0 & L_s \end{bmatrix}$$

The rotor voltage of the DFIG is the output voltage of a three-level T-type inverter, as shown in Fig. 4. Using Fortescue transformation and concerning phase voltages, we calculated the value in the rotor reference (*DQ*) frame as

$$u_{inv}^{DQ} = \frac{2}{3}\left(u_{AZ} + \lambda u_{BZ} + \lambda^2 u_{CZ}\right) \tag{5}$$

where $\lambda = e^{j2\pi/3} = -\frac{1}{2} + j\frac{\sqrt{3}}{2}$.

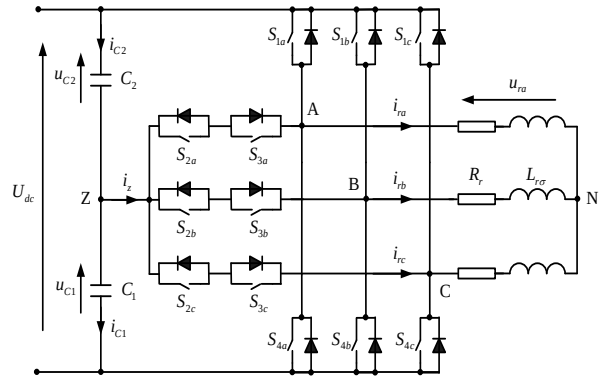

Fig. 4. Configuration of 3L-T-type inverter fed by DFIG

The output phase voltage u_{AZ}, u_{BZ}, and u_{CZ} of the 3L-T-type inverter is calculated via DC-link voltage U_{dc} and switching state S_x [5] as

$$u_{AZ} = S_a \frac{U_{dc}}{2}; u_{BZ} = S_b \frac{U_{dc}}{2}; u_{CZ} = S_c \frac{U_{dc}}{2} \tag{6}$$

where S_x indicates the switching state of each inverter phase: $S_x \in \{-1, 0, 1\}$ where $x \in \{a, b, c\}$.

The rotor voltage related to the stator side in the *dq* reference frame is obtained from (5) and (6) by using rotational coordinate transformation

$$u_r^{dq} = K u_{inv}^{DQ} e^{-j\theta_r} \tag{7}$$

where *K* implies the ratio between the stator and rotor voltages of the DFIG. θ_r is obtained from the stator flux angle θ_s and rotor angle θ_m.

Likewise, the rotor current referred to the stator side in the *dq* coordinate is obtained from its value in the rotor reference frame as

$$i_r^{dq} = \frac{1}{K} i_r^{DQ} e^{-j\theta_r} \tag{8}$$

If the DC-bus voltage is constant and $C_1 = C_2 = C$, the behavior of imaginary neutral-point voltage depends on the rotor currents of the DFIG and the switching states of the inverter [5, 16]

pISSN 1859-1388
eISSN 2615-9678

$$\frac{du_Z}{dt}=\frac{1}{2C}\left(2|S_a|-|S_b|-|S_c|\right)i_{Dr}+\frac{\sqrt{3}}{2C}\left(|S_b|-|S_c|\right)i_{Qr} \quad (9)$$

The CMV is determined from the voltage between the rotor neutral (N) and the midpoint of the DC-link (Z). It can be given as

$$u_{CMV}=\frac{1}{3}\left(u_{AZ}+u_{BZ}+u_{CZ}\right) \quad (10)$$

The stator active and reactive powers of the DFIG are given by [3, 7]

$$P_s=\frac{3}{2}\left(u_{ds}i_{ds}+u_{qs}i_{qs}\right)=\frac{3}{2}u_{ds}i_{ds}=\frac{3}{2}U_g i_{ds} \quad (11)$$
$$Q_s=\frac{3}{2}\left(u_{qs}i_{ds}-u_{ds}i_{qs}\right)=-\frac{3}{2}U_g i_{qs}$$

This equation indicates that we can control the active and reactive powers via the stator current.

Neglecting the power losses in the stator and rotor windings, we can express the rotor power in relation to the stator power as

$$P_r=-sP_s;Q_r=sQ_s \quad (12)$$

The discrete-time expression of the dynamic model is obtained by applying the first-order forward Euler's approximation approach for (4) during a sampling time T_{sp}

$$x(k+1)=A_e x(k)+B_e u(k) \quad (13)$$

where $A_e=e^{AT_{sp}}\simeq I+AT_{sp}$ (14)

$$B_e=\int_0^{T_{sp}} e^{A\left(T_{sp}-d\tau\right)}Bd\tau\simeq BT_{sp}$$

and I is a 3 × 3 identity matrix.

3 Proposed control strategy based on finite control set model predictive control approach

The purpose of the proposed control strategy based on model predictive control (MPDPC) is to

- track the generated active and reactive powers,
- maintain the balance of dc-bus voltage, and
- decrease the common-mode voltage.

For accomplishing these control objectives, the cost function of the 3L-T-type inverter fed by DFIG with computational delay compensation is formed as [14-17]

$$g\left(u_{k+1}\right)=\left(P_s^*(k+2)-P_s^p(k+2)\right)^2+\left(Q_s^*(k+2)-Q_s^p(k+2)\right)^2+\lambda_{uz}u_z^p(k+2)^2+\lambda_{cmv}u_{cmv}^p(k+2)^2 \quad (15)$$

where λ_{uz} and λ_{cmv} are the weighting factors of the DC-link voltage balancing and reduced CMV.

The future reference of stator active and reactive powers can be obtained by applying the second-order Lagrange extrapolation method

$$P_s^*(k+2)=6P_s^*(k)-8P_s^*(k-1)+3P_s^*(k-2)$$
$$Q_s^*(k+2)=6Q_s^*(k)-8Q_s^*(k-1)+3Q_s^*(k-2) \quad (16)$$

The control inputs of the system u_{dr} and u_{qr} are obtained from the sequence of switch state of the inverter $S_p=\begin{bmatrix}S_{pa} & S_{pb} & S_{pc}\end{bmatrix}^T$, indicated as a bounded finite set $S_p\in\{1,...,27\}$. Furthermore, each switching input S_{px} with $x\in\{a,b,c\}$ belongs to a compact set $\{-1,0,1\}$. Thus, the system is nonlinear, which is difficult to handle with the classical control method. Moreover, the capacitor voltage balancing and common-mode voltage of the proposed approach are solved regarding the cost function. Wherein, the classical method uses the complex modulation technique to maintain the balance of capacitor voltage and reduce the CMV. Consequently, the proposed control strategy provides more satisfying control performance and a simple control structure compared with the conventional method.

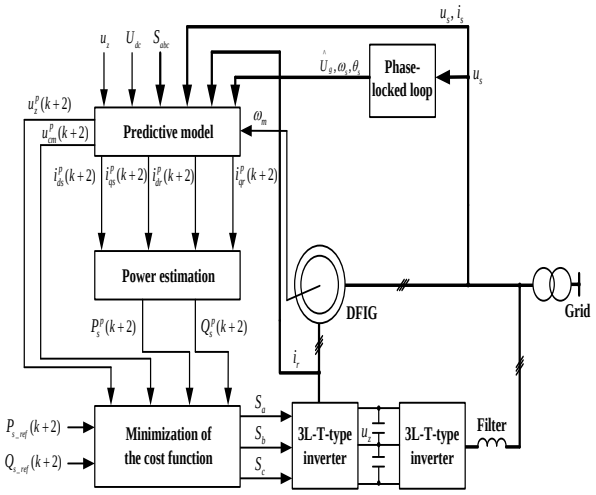

Fig. 5. Block diagram of proposed control strategy based on FCS-MPC

The control purposes of the proposed approach are illustrated in Fig. 5. The following steps give the summary of the proposed control strategy:

- Measure the stator and rotor currents, stator voltage and DC-link voltage,
- Calculate the predictive stator and rotor currents, neutral-point voltage, and common-mode voltage based on the predictive model,
- Compute the active and reactive powers,
- Evaluate and optimize the cost function, and
- Store the present value of switching state and apply the optimal switching states to the inverter.

4 Simulation results

The feasibility of the proposed control method was validated by using MATLAB/Simulink environment. Table 1 gives the parameters of the system analyzed.

Table 1. Parameters of the controllers and system

Parameter	Value	Description
P_s	2 [MW]	Rated stator active power
U_s	690 [V]	Line to line stator voltage
U_r	2070 [V]	Line to line rotor voltage
I_s	1760 [A]	Rated stator current
n_s	1500 [rpm]	Synchronous speed
p	2	The number pairs of poles
R_s	2.6 [mΩ]	Stator resistance
R_r	2.9 [mΩ]	Rotor resistance
$L_{\sigma s}$	87 [μH]	Stator leakage inductance
$L_{\sigma r}$	87 [μH]	Rotor leakage inductance
L_m	25 [mH]	Mutual inductance
f	50 [Hz]	Grid frequency
T_{sp}	100 [μs]	Sampling time of the controller
U_{dc}	1200 [V]	DC-link voltage
C	16 [μF]	DC-link capacitance

The mean absolute percentage error (MAPE) is utilized to evaluate the steady-state performance of the ripples for power tracking and capacitor voltage balancing

$$MAPE = \frac{1}{n}\sum_{i=1}^{n}\left|\frac{y_i^* - y_i}{y_i^*}\right|, \tag{17}$$

where y_i^* and y_i denote the desired value and measurement value.

For adjusting the power factor (PF) of the system, the desired value of stator reactive power is expressed by

$$Q_{s\_\mathrm{ref}} = P_{s\_\mathrm{ref}}\frac{\sqrt{1-PF^2}}{PF} \tag{18}$$

A comparison between the suggested method (MPDPC) and the conventional method

pISSN 1859-1388
eISSN 2615-9678

(PI controller) with space vector modulation (DPC-SVM) [3] was carried out for different operating conditions to verify the effectiveness of the proposed approach. The sampling time of the two controllers was fixed at 100 μs, corresponding to a switching frequency of 1 kHz. In this study, we performed two scenarios of the system analyzed. In the first case, several step-wise changes of stator active and reactive powers were examined under the conditions of synchronous speed. The initial values of the active power and power factor reference were –2 MW and PF = 1 at 0.5 s. The PF was switched from 1 to 0.9, from 0.9 to –0.9, and from –0.9 to 0.9 at 1, 1.5, and 2 s, respectively. The PF causes the reactive power references to step from 0 to –0.484 MVar at 1 s, from –0.484 to 0.484 MVar at 1.5 s, and from 0.484 to –0.727 MVar at 2 s.

Since the DFIG works at synchronous speed, the rotor's power is generally zero, as shown in Fig. 6. The simulation results show that we can achieve decoupled active and reactive powers control. As illustrated in Fig. 6c, the transient of stator active power accomplishes steady-state condition with 0.7 ms with the proposed approach and 0.9 ms for the DPC-SVM. Furthermore, the mean absolute percentage errors of active and reactive power for the DPC-SVM are 8.74 and 13.1%; whereas, they are 1.4 and 1.98% for the proposed method. Interestingly, the proposed technique exhibits improved control performance with a rapid dynamic response, smaller overshoot, and fewer power ripples compared with the DPC-SVM. The DPC-SVM has worse results principally because the dynamic of the inverter and especially the influence of the neutral point voltage variation are not considered in the control.

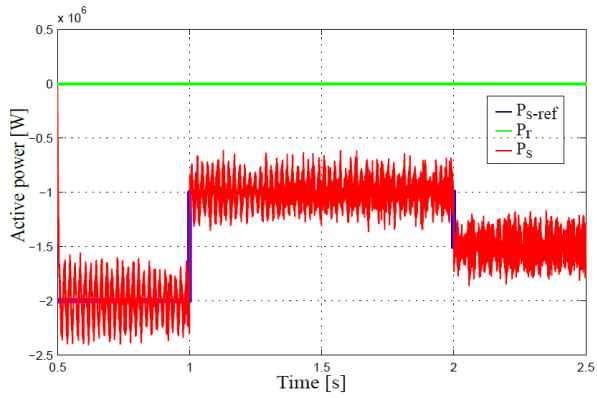

a) Generated active power of DPC-SVM

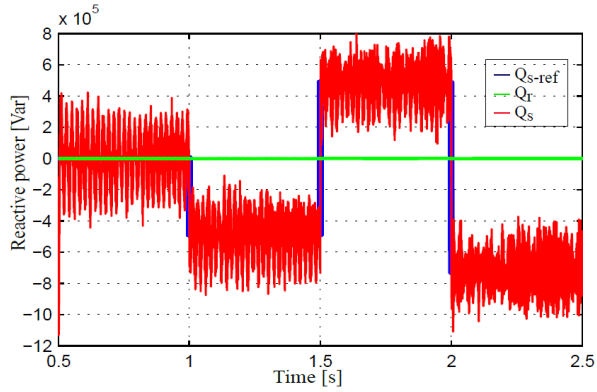

b) Generated reactive power of DPC-SVM

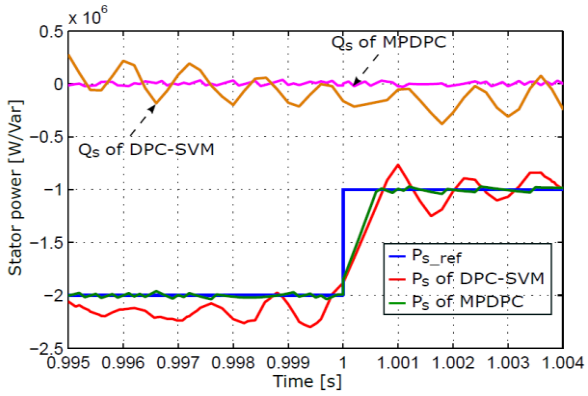

c) Dynamic response of active power with $Q_s = 0$

Fig. 6. Dynamic response of active and reactive power with synchronous speed for DPC-SVM

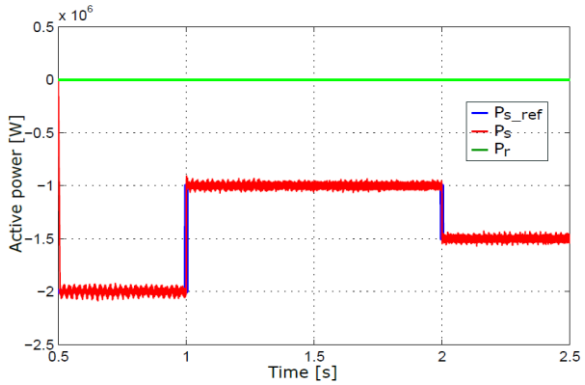

a) Generated active power of the proposed method

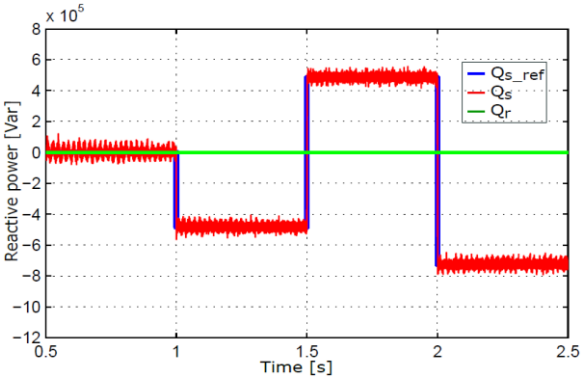

b) Generated reactive power of the proposed method

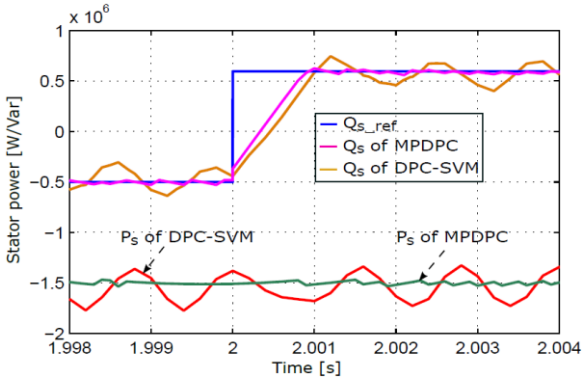

c) Transient response of reactive power with $P_s = -1.5$ MW

Fig. 7. Dynamic response of active and reactive power with synchronous speed for the proposed method

The THD of the stator current is under the 5% limit required according to the IEEE 519 standards. One of the severe drawbacks of the 3L-T-type inverter is the unbalance of DC-link capacitor voltage. Fig. 8 indicates that the DC-link capacitor voltages of the proposed method keep balanced with MAPE of neutral point voltages deviation 0.41% despite the transition of power references.

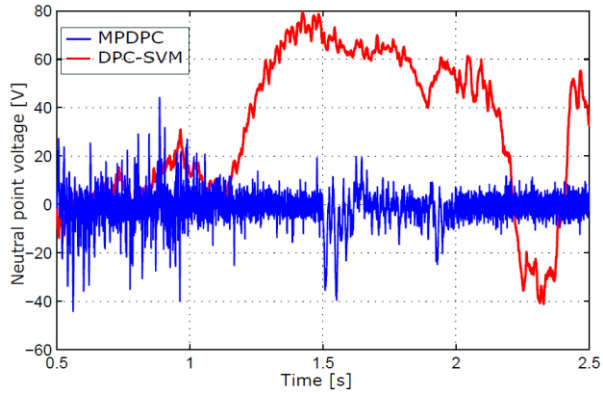

Fig. 8. Dynamic response of the neutral-point voltage for DPC-SVM and the proposed method

In the second situation, the rotor speed changed from 1200 to 1800 rpm during 0.5–2.2 s, as shown in Fig. 9a. A step-wise change of stator active power reference was implemented from −2 to −1 MW at 1.5 s and from −1 to −1.5 MW at 2 s, as demonstrated in Fig. 9b. In contrast, the reactive power reference was switched from –1.24 to 0.62 MVar at 1.5 s and from 0.62 to 0 Var at 2 s. It means that the power factor changed from 1 to a leading (0.85) or lagging (–0.85). When the rotor speed of the generator is greater than the synchronous speed, the slip is negative (s = –0.2). In this case, the rotor power, P_r , is transferred from the generator rotor to the grid via the rotor converters of the DFIG. Meanwhile, the RSC works as a rectifier and the GSC as an inverter. As shown in Figs. 9b and 9c, the powers delivered to the grid P_g and Q_g are the sums of the stator and rotor powers. In contrast, the DFIG slip is positive (s = 0.2) under the hyper-synchronous speed. This positive slip indicates that the rotor power is obtained from the grid through the converters. Here, the RSC operates as an inverter and the GSC as a rectifier. Notably, the proposed control strategy achieves satisfying dynamic performance during the sub- and hyper-synchronous operating modes.

pISSN 1859-1388
eISSN 2615-9678

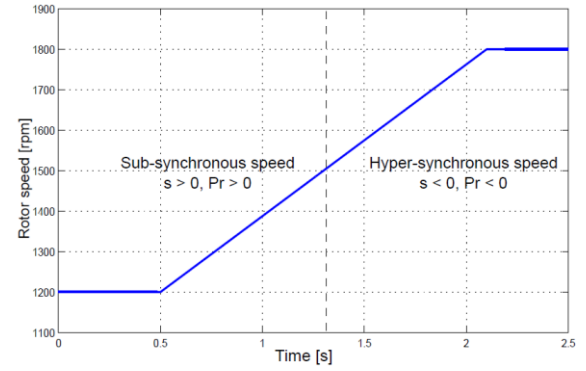

a) Response of rotor speed

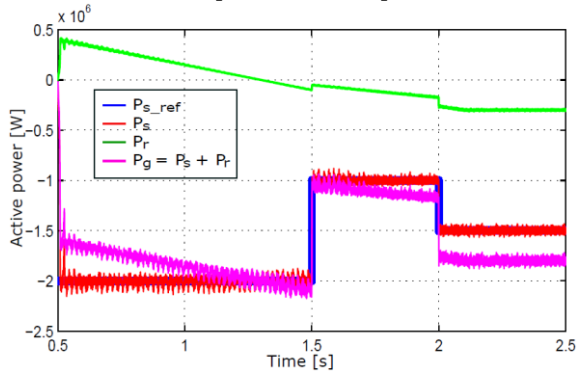

b) Generated active power

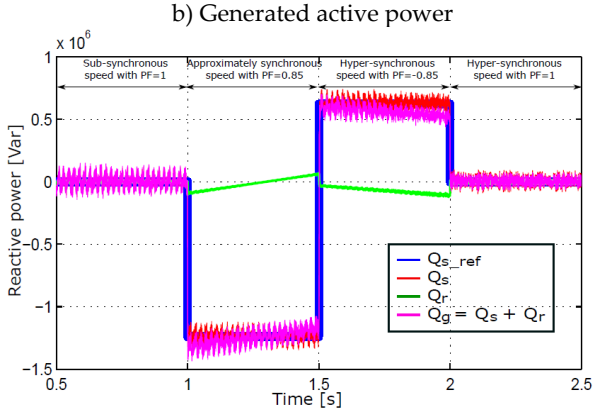

c) Generated reactive power

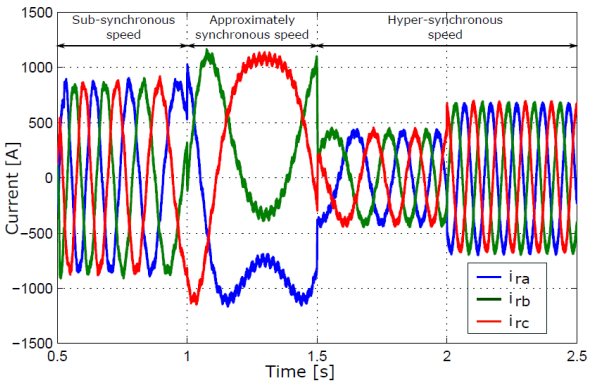

d) Rotor current

Fig. 9. Dynamic response of the proposed approach with rotor speed variation

On the contrary, a high common-mode voltage can cause overvoltage stress in the winding insulation of the electrical machine fed by the power converter, leading to deterioration and consequently reducing a lifetime of the machine. In our paper, this problem is resolved by considering the supplementary constraint CMV in the cost function. As can be seen in Fig. 10, the peak value of the CMV is reduced to 33.33% from $U_{dc}/2$ to $U_{dc}/3$ by choosing λ_{cmv} at 20 and 66.67% at 250.

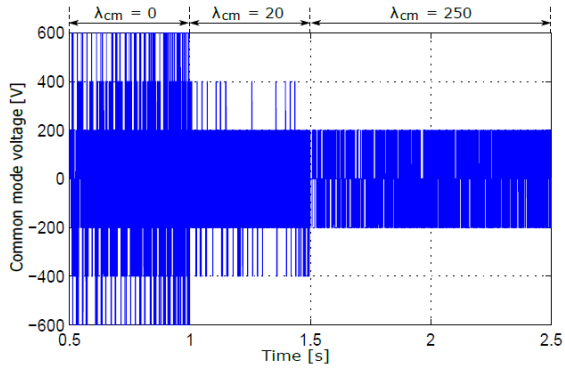

Fig. 10. Performance of the CMV

5 Conclusions

This paper presents an advanced strategy based on a model predictive control for a doubly-fed induction generator fed by a 3L-T-type inverter. The proposed approach allows to control bi-directionally transferred active and reactive powers, maintain the balance of the DC-link capacitor voltages, and decrease the common-mode voltage. A comparative study between the conventional control and the proposed method was carried out to validate the feasibility of the suggested strategy. The simulation results indicate that the proposed method exhibits more satisfying dynamic and static control performance than the classical controller. Furthermore, the control structure is simple because of the absence of the cascade control loop and modulation block.

Funding statement

This research was funded by Hue University under grant No. DHH2020-03-133.

References

1. Ma K, Tutelea L, Boldea I, Ionel DM, Blaabjerg F. Power electronic drives, controls, and electric generators for large wind turbines-an overview. Electric Power Compon Syst. 2015;43(12):1406-1421.
2. Blaabjerg F, Liserre M, Ma K. Power electronics converters for wind turbine systems. IEEE Transactions on Industry Applications. 2012;48(2):708-719.
3. Abad G, López J, Rodríguez MA, Marroyo L, Iwanski G. Doubly Fed Induction Machine. John Wiley & Sons, Inc;2011.
4. Schweizer M, Kolar JW. Design and implementation of a highly efficient three-level T-type converter for low-voltage applications. IEEE Trans Power Electron. 2013;28(2):899-907.
5. Ngo VQB, Nguyen MK, Tran TT, Lim YC, Choi JH. A simplified model predictive control for T-type inverter with output LC filter. Energies. 2019; 12(1):31.
6. Hopfensperger B, Atkinson DJ, Lakin RA. Stator-flux oriented control of a doubly-fed induction machine with and without position encoder. IEE Proceedings - Electric Power Applications. 2000;147(4):241-250.
7. Muller S, Deicke M, Doncker RWD. Doubly fed induction generator systems for wind turbines. IEEE Industry Applications Magazine. 2002;8(3):26-33.
8. Yang B, Jiang L, Wang L, Yao W, Wu Q. Nonlinear maximum power point tracking control and modal analysis of DFIG based wind turbine. International Journal of Electrical Power & Energy Systems. 2016;74:429-436.
9. Prasad RM, Mulla MA. Rotor Position-Sensorless Algorithms for Direct Power Control of Rotor-Tied DFIG. IEEE Transactions on Power Electronics. 2021;36(6):6213-6217.
10. Hu J, Yuan X. VSC-based direct torque and reactive power control of doubly-fed induction generator. Renewable Energy. 2012;40:13-23.
11. Xiong L, Wang J, Mi X, Khan MW. Fractional order sliding mode based direct power control of grid-connected DFIG. IEEE Transactions on Power Systems. 2018;33(3):3087-3096.
12. Hu J, Li Y, Zhu J. Multi-objective model predictive control of doubly-fed induction generators for wind energy conversion. IET Generation Transmission Distribution. 2019;13(1):21-29.
13. Kou P, Liang D, Li J, Gao L, Ze Q. Finite-Control-Set Model Predictive Control for DFIG Wind Turbines. IEEE Transactions on Automation Science and Engineering. 2018;15(3):1004-13.
14. Rodriguez J, Kazmierkowski MP, Espinoza JR, Zanchetta P, Abu-Rub H, Young HA, et al. State of the art of finite control set model predictive control in power electronics. IEEE Transactions on Industrial Informatics. 2013;9(2):1003-1016.
15. Abdelrahem M, Kennel R. Efficient direct model predictive control for doubly-fed induction generators. Electric Power Components and Systems. 2017;45(5):574-87.
16. Rodriguez J, Cortes P. Predictive control of power converters and electrical drives. John Wiley & Sons, Inc;2012.
17. Kouro S, Cortes P, Vargas R, Ammann U, Rodriguez J. Model predictive control-a simple and powerful method to control power converters. IEEE Transactions on Industrial Electronics. 2009;56(6):1826-38.
18. Rafiee Z, Heydari R, Rafiee M, Aghamohammadi MR, Rodriguez J, Blaabjerg F, editors. Adaptive Model Predictive Control of DFIG-based Wind Farm: A Model-Free Control Approach. 2020 IEEE 21st Workshop on Control and Modeling for Power Electronics (COMPEL); 2020 9-12 Nov. 2020.
19. Mossa MA, Do TD, Al-Sumaiti AS, Quynh NV, Diab AAZ. Effective Model Predictive Voltage Control for a Sensorless Doubly Fed Induction Generator. IEEE Canadian Journal of Electrical and Computer Engineering. 2021;44(1):50-64.